articles

molecular pharmaceutics

Cellular Uptake and Nanoscale Localization of Gold Nanoparticles in Cancer Using Label-Free Confocal Raman Microscopy

Neha B. Shah,[†] Jinping Dong,[‡] and John C. Bischof*[,†,§]

Department of Biomedical Engineering, Characterization Facility, and Department of Mechanical Engineering, University of Minnesota, Minneapolis, Minnesota 55455, United States

Received August 5, 2010; Revised Manuscript Received October 21, 2010; Accepted November 5, 2010

Abstract: This work demonstrates the use of confocal Raman microscopy (CRM) to measure the dynamics of cellular uptake and localization of gold nanoparticles (GNP) with nanoscale resolution. This is important as nanoparticle cellular interactions are increasingly under investigation to support applications as diverse as drug delivery, gene transfection and a variety of heat and radiation based therapeutics. At the heart of these applications is a need to know the dynamics of nanoparticle cellular uptake and localization (i.e., cell membrane, cytoplasm or nucleus). This process can change dramatically based on size, charge, shape and ligand attached to the nanoparticle. While electron microscopy, atomic emission spectroscopy and histology can be used to assess cellular uptake, they are labor intensive and post-mortem and can miss critical dynamics of the process. For this reason investigators are increasingly turning to optically active nanoparticles that allow direct microscopic interrogation of uptake. Here we show that CRM adds to this evolving armamentarium as a fast, noninvasive, and label-free technique to dynamically study cellular uptake of GNPs with subcellular detail in cancer. Raman laser interaction with GNPs inside cells shows unique spectroscopic features corresponding to the intracellular localization of GNPs over 2 to 24 h at the membrane, cytoplasm or nucleus that are separately verified by histology (silver staining) and electron microscopy. These results show that CRM has the potential to facilitate high-throughput study of the dynamics and localization of a variety of GNPs in multiple cell types.

Keywords: Confocal microscopy; Raman spectroscopy; drug delivery; therapeutics; gold nanoparticles; cellular uptake; cellular localization; label-free detection; cancer

Introduction

There has been a veritable explosion of research and development of nanoparticle (NP) based diagnostics and therapeutics in recent years.[1−7] As therapeutic delivery vehicles (i.e., carriers of drug, gene, siRNA, etc.) or as therapeutic agents themselves, NPs offer high efficiency and selectivity as well as reduced systemic toxicity. Of these, gold-based NPs are among the most intensively studied due to their optical properties, relatively inert status in the body,

* Corresponding author. Mailing address: University of Minnesota, Departments of Mechanical Engineering, Biomedical Engineering, and Urologic Surgery, Mechanical Engineering 1100, 111 Church St SE, Minneapolis, MN 55455. Phone: 612-625-5513. Fax: 612-625-4344. E-mail: bischof@umn.edu.

[†] Department of Biomedical Engineering.

[‡] Characterization Facility.

[§] Department of Mechanical Engineering.

(1) Riehemann, K.; Schneider, S. W.; Luger, T. A.; Godin, B.; Ferrari, M.; Fuchs, H. Nanomedicine—Challenge and Perspectives. *Angew. Chem., Int. Ed.* **2009**, *48* (5), 872–897.

(2) Murday, J. S.; Siegel, R. W.; Stein, J.; Wright, J. F. Translational nanomedicine: status assessment and opportunities. *Nanomedicine* **2009**, *5* (3), 251–273.

(3) Emily, S. D.; Jennifer, G. M.; Jennifer, L. W. Nanoparticles for Thermal Cancer Therapy. *J. Biomech. Eng.* **2009**, *131* (7), 074001.

(4) Zamboni, W. C. Concept and Clinical Evaluation of Carrier-Mediated Anticancer Agents. *Oncologist* **2008**, *13* (3), 248–260.

10.1021/mp1002587
Published on Web 11/05/2010

unique nanoscale properties, ease with which surface chemistry can be altered, and commercial availability in different sizes and shapes. Two specific examples include Aurimmune, a GNP that delivers the therapeutic tumor necrosis factor (TNF),[8] and Auroshell, a gold-silica core−shell NP that itself functions as a therapeutic by enhancing laser absorption and thereby heating within tumors.[9] In short, there are many examples of GNP therapeutics under development.[10−14] In some cases, the GNP is delivering a drug payload to a membrane receptor or perhaps internally to a cytoplasmic (i.e., cytoskeletal) target.[13] In other cases the nanoparticle is targeted to the membrane to enhance cell lysis during laser heating or targeted to the nucleus to enhance scattered radiation to increase DNA strand breaks.[15−17] Clearly, the dynamics of loading and localization of the GNP within the cell are critical to many applications including drug delivery and therapeutics.

In the past few years, the interactions of GNPs with a variety of cell systems have been investigated to describe uptake mechanisms, intracellular distribution and downstream effects such as toxicity, cell cycle regulation etc. It has been shown that GNPs of various sizes (1−100 nm) and shapes (spherical, shells, rods, diamonds) can be taken up in a variety of cell types.[18−24] The degree of uptake, cellular distribution and toxicity of these GNPs depends upon and would further vary due to surface ligand or therapeutic agent. Often GNP uptake studies utilize labor intensive and high-resolution methods such as transmission electron microscopy (TEM) in order to understand the subcellular distribution of GNPs down to cellular organelle scale. Chithrani et al. have shown using TEM that GNPs of various sizes ranging from 14 to 74 nm are found in cell cytoplasm in ∼500 nm size vesicles (endosomes that later fuse with lysosomes) that contain multiple GNPs.[21] The number of GNPs per vesicle and thus per cell can be quantified using techniques such as inductively coupled plasma mass spectrometry (ICP-MS) or atomic emission spectroscopy (AES), which require digestion of the cells and analysis of total gold per sample. An ICP-MS study in human colon cancer cells showed that uptake of gold nanorods varies from 50 to 2300 particles per cell depending upon the surface chemistry with surfactant coated rods showing the least uptake and highest toxicity.[25] A similar study conducted with AES showed that spherical nanoparticles of size 50 nm show the highest uptake in HeLa cells compared to other sizes and gold nanorods. These two methods combined with uptake inhibitor studies have also clarified uptake mechanisms of GNPs which vary from receptor mediated clathrin-dependent endocytosis to macropinocytosis depending upon surface chemistry, shape, GNP size and cell type tested.[19,26,27] Though these methods are important for in-depth quantification and classification of uptake mechanisms of certain basic GNPs, quick methods

(5) Jain, P. K.; Huang, X.; El-Sayed, I. H.; El-Sayed, M. A. Noble Metals on the Nanoscale: Optical and Photothermal Properties and Some Applications in Imaging, Sensing, Biology, and Medicine. *Acc. Chem. Res.* **2008**, *41* (12), 1578–1586.

(6) Jain, P. K.; El-Sayed, I. H.; El-Sayed, M. A. Au nanoparticles target cancer. *Nano Today* **2007**, *2* (1), 18–29.

(7) Fischer, H. C.; Chan, W. C. W. Nanotoxicity: the growing need for in vivo study. *Curr. Opin. Biotechnol.* **2007**, *18* (6), 565–571.

(8) Paciotti, G. F.; Myer, L.; Weinreich, D.; Goia, D.; Pavel, N.; McLaughlin, R. E.; Tamarkin, L. Colloidal Gold: A Novel Nanoparticle Vector for Tumor Directed Drug Delivery. *Drug Delivery* **2004**, *11* (3), 169–183.

(9) Stern, J. M.; Stanfield, J.; Kabbani, W.; Hsieh, J.-T.; Cadeddu, J. A. Selective Prostate Cancer Thermal Ablation With Laser Activated Gold Nanoshells. *J. Urol.* **2008**, *179* (2), 748–753.

(10) Nanospectra, http://www.nanospectra.com/technology/aurolase-therapy.html. 2009.

(11) Cytimmune, http://www.cytimmune.com/go.cfm?do=Page.View&pid=26. 2009.

(12) Shan, J.; Tenhu, H. Recent advances in polymer protected gold nanoparticles: synthesis, properties and applications. *Chem. Commun.* **2007**, (44), 4580–4598.

(13) Han, G.; Ghosh, P.; Rotello, V. M. Functionalized gold nanoparticles for drug delivery. *Nanomedicine* **2007**, *2* (1), 113–123.

(14) Bergen, J. M.; Recum, H. A. v.; Goodman, T. T.; Massey, A. P.; Pun, S. H. Gold Nanoparticles as a Versatile Platform for Optimizing Physicochemical Parameters for Targeted Drug Delivery. *Macromol. Biosci.* **2006**, *6* (7), 506–516.

(15) Zharov, V. P.; Mercer, K. E.; Galitovskaya, E. N.; Smeltzer, M. S. Photothermal Nanotherapeutics and Nanodiagnostics for Selective Killing of Bacteria Targeted with Gold Nanoparticles. *Biophys. J.* **2006**, *90* (2), 619–627.

(16) Kong, T.; Zeng, J.; Wang, X.; Yang, X.; Yang, J.; McQuarrie, S.; McEwan, A.; Roa, W.; Chen, J.; Xing, J. Z. Enhancement of Radiation Cytotoxicity in Breast-Cancer Cells by Localized Attachment of Gold Nanoparticles. *Small* **2008**, *4* (9), 1537–1543.

(17) Hainfeld, J. F.; Dilmanian, F. A.; Slatkin, D. N.; Smilowitz, H. M. Radiotherapy enhancement with gold nanoparticles. *J. Pharm. Pharmacol.* **2008**, *60* (8), 977–985.

(18) Arvizo, R. R.; Miranda, O. R.; Thompson, M. A.; Pabelick, C. M.; Bhattacharya, R.; Robertson, J. D.; Rotello, V. M.; Prakash, Y. S.; Mukherjee, P. Effect of Nanoparticle Surface Charge at the Plasma Membrane and Beyond. *Nano Lett.* **2010**, *10* (7), 2543–2548.

(19) Chithrani, B. D.; Chan, W. C. Elucidating the mechanism of cellular uptake and removal of protein-coated gold nanoparticles of different sizes and shapes. *Nano Lett.* **2007**, *7* (6), 1542–1550.

(20) Chithrani, B. D.; Ghazani, A. A.; Chan, W. C. W. Determining the Size and Shape Dependence of Gold Nanoparticle Uptake into Mammalian Cells. *Nano Lett.* **2006**, *6* (4), 662–668.

(21) Chithrani, B. D.; Stewart, J.; Allen, C.; Jaffray, D. A. Intracellular uptake, transport, and processing of nanostructures in cancer cells. *Nanomedicine* **2009**, *5* (2), 118–127.

(22) Pan, Y.; Neuss, S.; Leifert, A.; Fischler, M.; Wen, F.; Simon, U.; Schmid, G.; Brandau, W.; Jahnen-Dechent, W. Size-dependent cytotoxicity of gold nanoparticles. *Small* **2007**, *3* (11), 1941–1949.

(23) Patra, H. K.; Banerjee, S.; Chaudhuri, U.; Lahiri, P.; Dasgupta, A. K. Cell selective response to gold nanoparticles. *Nanomedicine* **2007**, *3* (2), 111–119.

(24) Murphy, C. J.; Gole, A. M.; Stone, J. W.; Sisco, P. N.; Alkilany, A. M.; Goldsmith, E. C.; Baxter, S. C. Gold Nanoparticles in Biology: Beyond Toxicity to Cellular Imaging. *Acc. Chem. Res.* **2008**, *41* (12), 1721–1730.

(25) Alkilany, A. M.; Nagaria, P. K.; Hexel, C. R.; Shaw, T. J.; Murphy, C. J.; Wyatt, M. D. Cellular Uptake and Cytotoxicity of Gold Nanorods: Molecular Origin of Cytotoxicity and Surface Effects. *Small* **2009**, *5* (6), 701–708.

that allow screening of cellular binding and uptake of a library of GNPs are increasingly needed.

More recently, faster noninvasive optical methods for GNP uptake assessment have been developed. Most of these techniques rely on the plasmonic properties of GNPs including surface enhanced Raman scattering (SERS), dark field, two-photon luminescence (TPL), multimodal photoacoustic, Rayleigh light scattering and total internal reflection (TIR) fluorescence microscopy.[24,28−35] Some of these techniques are easy to set up such as dark field, TIR and Rayleigh light scattering, but provide limited spatial resolution (few micrometers) and sensitivity. SERS can provide high sensitivity but requires GNP surface labeling with SERS active molecules, which in turn would affect the uptake and intracellular distribution of GNPs. Thus, there remains the need for a higher resolution label-free optical technique to assess GNP uptake and localization within cells.

The present work shows that confocal Raman microscopy (CRM) can be used as a fast, noninvasive, and label-free technique to dynamically study cellular binding and uptake of GNPs with subcellular detail in cancer cells (~250 nm spatial resolution). Raman laser interaction with GNPs inside cells shows unique spectroscopic features corresponding to the intracellular localization of GNPs over 2 to 24 h. The results were confirmed using AES, histology and TEM and are comparable to previously reported cellular uptake studies of GNPs. Our findings suggest that CRM has the potential to be a high-throughput tool to study the effect of physicochemical parameters (charge, coating, targeting) of GNPs on their binding, uptake and intracellular localization in a variety of cellular systems.

Materials and Methods

Gold Nanoparticles. GNPs 30 nm in diameter and spherical in shape, with surface coating of polyethylene glycol (PEG, 5000 MW), were a gift from CytImmune Sciences, Inc. (Rockville, MD).

Cell Culture. Human prostate cancer LNCaP Pro 5 cells were grown as adherent monolayers in 6-well plates (Costar) on sterilized glass coverslips (22 × 22 mm). Cells were maintained in Dulbecco's modified Eagle's medium (DMEM)/F12 (Invitrogen) supplemented with 10% fetal bovine serum (FBS) (Invitrogen), 5% penicillin/streptomycin, and 10^{-9} M dihydrotestosterone (DHT) (Sigma). Cells were incubated in a 37 °C humidified incubator with 5% CO_2 and were allowed to grow up to 48 h (70% confluency). Cells were then treated with GNPs for 2, 12, and 24 h at 37 °C. At the end of incubation, the cells were washed thoroughly by dipping the coverslip 20 times in each of three beakers of 1× phosphate buffered saline (PBS). The glass coverslip was then inverted over another coverslip with spacers (0.17 mm thick). All air bubbles were carefully removed and the sandwich of coverslips was sealed with silicone grease to prevent dehydration during measurements.

Confocal Raman Microscopy (CRM). Cell imaging was performed with a WITech alpha 300R Confocal Raman Microscope (Ulm, Germany) at room temperature. An air-cooled argon-ion laser operating at $\lambda = 514.5$ nm was used as an excitation source with the output power varying between 2−20 mW. A Nikon Fluor (100×/1.25 NA) oil immersion objective was used to collect Raman spectra from single cells. The optical resolution with such setup reaches ~250 nm in the x and y directions, and ~500 nm in the vertical direction. Cells sandwiched between two glass coverslips (with PBS and sealed with grease) were mounted on a piezoelectric scanning stage. The objective was brought into contact with the oil drop placed on the top piece of the coverslip during scanning (the cells were attached to the bottom surface of the top piece of the coverslip). A 2D array of Raman spectra (i.e., 100 × 100 pixels for all $x-y$ images presented here) were recorded when the sample was raster-scanned on a selected area. The integration time for each spectrum was controlled to be the same at each pixel and was 0.1 s for all scans. Chemical maps (images) were generated by integrating one or more characteristic Raman peaks and rendering the peak intensity as brightness at each pixel location. Images generated from the C−H peak (organic components) at 2800−3100 cm^{-1} were used to show the basic cell structure, and the contrast generated from the broad photoluminescence (PL) peak between 180 and 1800 cm^{-1} was used to show the localization of GNPs. Two to three cells were randomly selected under bright field for each experimental setup. A depth scan ($x-z$ direction) across the

(26) Dobrovolskaia, M. A.; McNeil, S. E. Immunological properties of engineered nanomaterials. *Nat. Nano* **2007**, *2* (8), 469–478.
(27) Shukla, R.; Bansal, V.; Chaudhary, M.; Basu, A.; Bhonde, R. R.; Sastry, M. Biocompatibility of Gold Nanoparticles and Their Endocytotic Fate Inside the Cellular Compartment: A Microscopic Overview. *Langmuir* **2005**, *21* (23), 10644–10654.
(28) El-Sayed, I. H.; Huang, X.; El-Sayed, M. A. Surface Plasmon Resonance Scattering and Absorption of anti-EGFR Antibody Conjugated Gold Nanoparticles in Cancer Diagnostics: Applications in Oral Cancer. *Nano Lett.* **2005**, *5* (5), 829–834.
(29) Galanzha, E. I.; Shashkov, E. V.; Kelly, T.; Kim, J.-W.; Yang, L.; Zharov, V. P. In vivo magnetic enrichment and multiplex photoacoustic detection of circulating tumour cells. *Nat. Nano* **2009**, *4* (12), 855–860.
(30) He, H.; Xie, C.; Ren, J. Nonbleaching Fluorescence of Gold Nanoparticles and Its Applications in Cancer Cell Imaging. *Anal. Chem.* **2008**, *80* (15), 5951–5957.
(31) Louit, G.; Asahi, T.; Tanaka, G.; Uwada, T.; Masuhara, H. Spectral and 3-Dimensional Tracking of Single Gold Nanoparticles in Living Cells Studied by Rayleigh Light Scattering Microscopy. *J. Phys. Chem. C* **2009**, *113* (27), 11766–11772.
(32) Lee, S.; Kim, S.; Choo, J.; Shin, S. Y.; Lee, Y. H.; Choi, H. Y.; Ha, S.; Kang, K.; Oh, C. H. Biological Imaging of HEK293 Cells Expressing PLCγ1 Using Surface-Enhanced Raman Microscopy. *Anal. Chem.* **2007**, *79* (3), 916–922.
(33) Huff, T. B.; Tong, L.; Zhao, Y.; Hansen, M. N.; Cheng, J.-X.; Wei, A. Hyperthermic effects of gold nanorods on tumor cells. *Nanomedicine* **2007**, *2* (1), 125–132.
(34) Tong, L.; Zhao, Y.; Huff, T. B.; Hansen, M. N.; Wei, A.; Cheng, J.-X. Gold Nanorods Mediate Tumor Cell Death by Compromising Membrane Integrity. *Adv. Mater.* **2007**, *19* (20), 3136–3141.
(35) Axelrod, D. Total Internal Reflection Fluorescence Microscopy. In *Methods in Cell Biology*; Correia, J. J., Detrich, H. W., III, Eds.; Academic Press: 2008; Vol. 89, Chapter 7, pp 169−221.

cell was usually performed first to show the cross section of the cell. The lateral scan ($x-y$ direction) was then performed based on the depth scan. For each time point, the experiment was repeated three times and at least two to three cells were imaged per experiment.

Atomic Emission Spectroscopy (AES). Cells were treated with the GNPs as above and then digested with 5 mL of aqua regia (4 parts HNO_3 + 1 part HCl). Aliquots of this solution were mixed with an internal standard and analyzed by comparing them to a calibration curve constructed using multielement standards for gold quantification.

Transmission Electron Microscopy (TEM). TEM processing was performed on cell monolayers at 24 h after incubation with GNPs. Monolayers were fixed in 2% glutaraldehyde/0.1 M sodium cacodylate buffer for 1 h, postfixed in 2% osmium tetroxide for 2 h, and dehydrated in graded concentrations of ethanol and propylene oxide. Cell samples were then embedded in Epon (Polysciences Inc., PA) and thin-sectioned. Sections of 60−70 nm thickness were collected on 250 mesh Formvar copper grids (Ted Pella, CA) and stained with a 1:1 mix of methanol and lead citrate. The grids were visualized under a JEOL 1200 transmission electron microscope (Hitachi, Japan) at 80 kV.

Histology. Cells treated with GNPs were trypsinized, washed and fixed in 10% formalin for 30 min. Samples were centrifuged at 1800 rpm for 10 min. Supernatant was removed, and pellet was embedded in paraffin using HistoGel. The paraffin blocks were sectioned with a thickness of about 3 μm and collected on uncharged glass slides. The sections were dewaxed and stained with LI Silver (Nanoprobes Inc., Yaphank, NY). The slides were then counterstained with nuclear Fast Red. Light microscopy images were taken with a Nikon optical microscope with a 100× oil immersion objective.

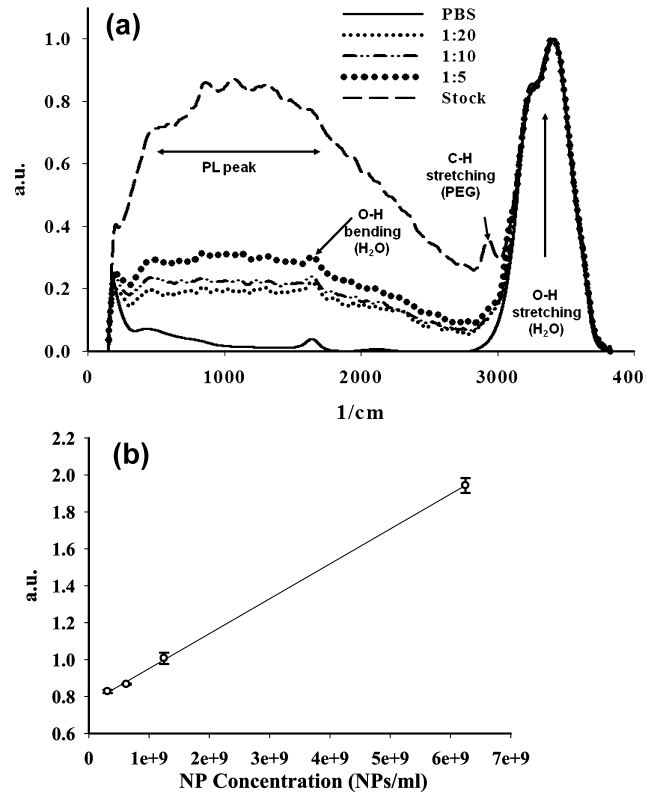

Figure 1. Plasmon emission peak changes as a function of GNP concentration. (a) Raman spectra of GNP solutions at different concentrations. Each spectrum shown is an average of ten. (b) Raman calibration of GNPs in solution. Area under the curve for the PL peak (180−1800 cm^{-1}) is plotted against the concentration of GNP solutions. GNP solutions were prepared using serial dilution of the stock in DI water. Concentration of the stock is 6.25 × 10^9 GNPs/mL. The graph shows data for stock, 1:5, 1:10, and 1:20 dilution. Linear fit (R^2 = 0.999).

Results

GNPs can be tracked on the basis of their photoluminescence (PL) peak (180−1800 cm^{-1}) attributable to the excitation of their surface plasmons by Raman laser.[36] A stock solution of 30 nm PEG coated GNPs gives a broad PL peak as indicated in Figure 1a. The intensity of this peak decreases with increasing dilution of the stock solution (Figure 1a, 1:20−1:5). This change in PL peak intensity shows a linear correlation with the concentration of the GNPs (Figure 1b). Additionally, various molecules in a biological cell (i.e., proteins, lipids, nucleic acids) give distinct Raman peaks in the spectral range of 500−3500 cm^{-1}.[37−39] Cellular organelles (i.e., membrane, nucleus, mitochondria) can be imaged based on these functional groups specific to them without the use of stains or dyes.[37,38,40] Thus, the characteristic PL peak of GNPs can be used to locate and monitor their uptake relative to cellular constituents.

Uptake studies were performed with 30 nm PEG coated GNPs on LNCaP pro5, human prostate cancer cells. Cells were allowed to grow and attach to glass coverslips to facilitate corroborative bright field measurement of cell dimensions. Figure 2a shows a bright field image of a cell, based on which a depth scan was performed by CRM. A depth scan allows the assessment of attachment site of the

(36) Govorov, A. O.; Richardson, H. H. Generating heat with metal nanoparticles. *Nano Today* **2007**, *2* (1), 30–38.

(37) Movasaghi, Z.; Rehman, S.; Rehman, I. U. Raman Spectroscopy of Biological Tissues. *Appl. Spectrosc. Rev.* **2007**, *42*, 493–541.

(38) Matthaus, C.; Kale, A.; Chernenko, T.; Torchilin, V.; Diem, M. New Ways of Imaging Uptake and Intracellular Fate of Liposomal Drug Carrier Systems inside Individual Cells, Based on Raman Microscopy. *Mol. Pharmaceutics* **2008**, *5* (2), 287–293.

(39) Zhang, D.; Neumann, O.; Wang, H.; Yuwono, V. M.; Barhoumi, A.; Perham, M.; Hartgerink, J. D.; Wittung-Stafshede, P.; Halas, N. J. Gold Nanoparticles Can Induce the Formation of Protein-based Aggregates at Physiological pH. *Nano Lett.* **2009**, *9* (2), 666–671.

(40) Uzunbajakava, N.; Lenferink, A.; Kraan, Y.; Volokhina, E.; Vrensen, G.; Greve, J.; Otto, C. Nonresonant Confocal Raman Imaging of DNA and Protein Distribution in Apoptotic Cells. *Biophys. J.* **2003**, *84* (6), 3968–3981.

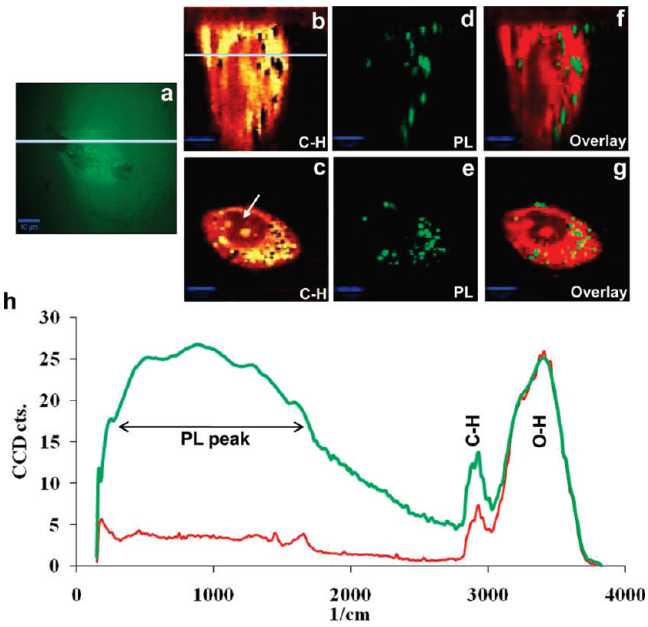

Figure 2. CRM scanning at single cell level. (a) An optical image of the cell (top view). Line indicates the location where CRM scanning was performed. (b) CRM depth scan of the cell (showing thickness of the cell). The top surface is attached to the glass coverslip. The line indicates the depth where the lateral scan (c) was performed. (c) CRM lateral scan of the cell. Nucleus (arrow) and nucleoli (bright spots within the nucleus) are clearly visible. (d, e) CRM scans of GNPs generated with PL peak showing GNP as green spots. Panels d and e correspond to cell images in b and c respectively. (f, g) Overlay of the depth and lateral cell images (b, c) with their corresponding GNP images (d, e). The overlays show relative location of GNPs (green) within the cell (red). (h) Representative Raman spectra of the cell. Green and red curves show typical spectra within a cell with and without GNP respectively. Panels b and c constructed from integration of the C−H peak; panels d and e constructed from integration of the PL peak; panels f and g, pseudo color overlays. (Scale bars = 5 μm.)

cell to the glass coverslip and the thickness of the cell. A typical LNCaP depth scan (60 × 60 pixels) is shown in Figure 2b based on the integration of a group of peaks between 2800 and 3100 cm^{-1} (Figure 2h) that result from C−H stretching vibrations native to cellular organic content.[37] Based on the depth scan image, single (or multiple) lateral scans, such as Figure 2c, of the same cell can be performed (taken along the line in Figure 2b). Figure 2c is also constructed based on C−H stretching vibrations. When GNPs are present in a cell, the Raman spectrum (green in Figure 2h) is augmented by the PL peak (180−1800 cm^{-1}), which can be integrated to generate an image of GNP distribution (Figure 2d,e). By overlaying C−H (Figure 2b,c, red spectrum) and PL (Figure 2d,e, green spectrum) images, the localization of GNPs within the cells becomes clear (Figure 2f,g). Each green spot (= single or clustered GNPs) has a variable intensity and size. The spot size is limited by the Raman spatial resolution (~250 nm) while the intensity appears to be correlated to the number of GNPs present (Figure 4e, Figure 1b).

Cellular uptake was evaluated with CRM at three time points. For each time point, an experiment was carried out at least 3 times in at least 2 or 3 cells. Figure 3 shows CRM scans for this study. Overlay images for depth scans (indicated with "D") and their corresponding lateral scans (indicated with "L", taken at the center of the depth scan) for three cells at each 2, 12, and 24 h time points are shown. At 2 h, most GNPs were found to be at the cell periphery as seen in cells L1a and L2a (Figure 3), with very little intracellular uptake (L3a of Figure 3). At 12 h, the cells showed higher uptake of GNPs compared to 2 h with GNP clusters distributed throughout the cytoplasm. This can be seen in both small and large cells (Figure 3, cells L1b and L2b) as well as in a dividing cell (cell L3b) and is consistent with previous reports of GNP internalization.[41,42] The cellular uptake of GNPs continued to increase from 12 to 24 h, with growing cluster size and localization near the nucleus. This is in agreement with the histology and TEM data (Figure 4). Figure 4a−c shows histology images of LNCaP cells treated with GNPs for 2, 12, and 24 h. Silver enhancement was used to identify localization of GNPs in the histological sections of LNCaP cells. Silver enhancement deposits metallic silver on top of GNPs until it becomes visible in light microscopy as a black stain. As shown in Figure 4a, GNP treated LNCaP cells show a faint black border (silver stain) at the cell membrane for the 2 h treatment. At 12 h, silver stain appears in the cytoplasm indicating intracellular accumulation of GNPs (Figure 4b), which agrees with CRM scans (Figure 3, 12 h). At 24 h, large deposits of silver stain appear at the periphery of the nucleus (Figure 4c) with TEM (Figure 4d) showing multiple membrane bound vesicles (each with 3−15 GNPs) accumulating in the perinuclear region. The uptake kinetics and intracellular distribution of GNPs in this study are consistent with the pinocytotic pathway of endocytosis of nontargeted (i.e., PEGylated) GNPs.[27]

Quantitative AES results show that there are about 19.9 ± 0.97, 28.0 ± 0.44, 284 ± 5.5 GNPs per cell at 2, 12, and 24 h respectively. Cellular uptake does not reach saturation as shown in Figure 4e (AES data). An integrated density analysis of the PL images (i.e., Figure 2d,e) at 2, 12, and 24 h, using ImageJ, shows a similar trend in uptake as AES (Figure 4e). As GNPs aggregate within cells (as shown in TEM of Figure 4d), the interactions among the particles may affect the plasmon excitation, which may not give a linear correlation between PL peak intensity and the number of

(41) Lapotko, D. O.; Lukianova-Hleb, E. Y.; Oraevsky, A. A. Clusterization of nanoparticles during their interaction with living cells. *Nanomedicine* **2007**, *2* (2), 241–253.

(42) Myllynen, P. K.; Loughran, M. J.; Howard, C. V.; Sormunen, R.; Walsh, A. A.; Vähäkangas, K. H. Kinetics of gold nanoparticles in the human placenta. *Reprod. Toxicol.* **2008**, *26* (2), 130–137.

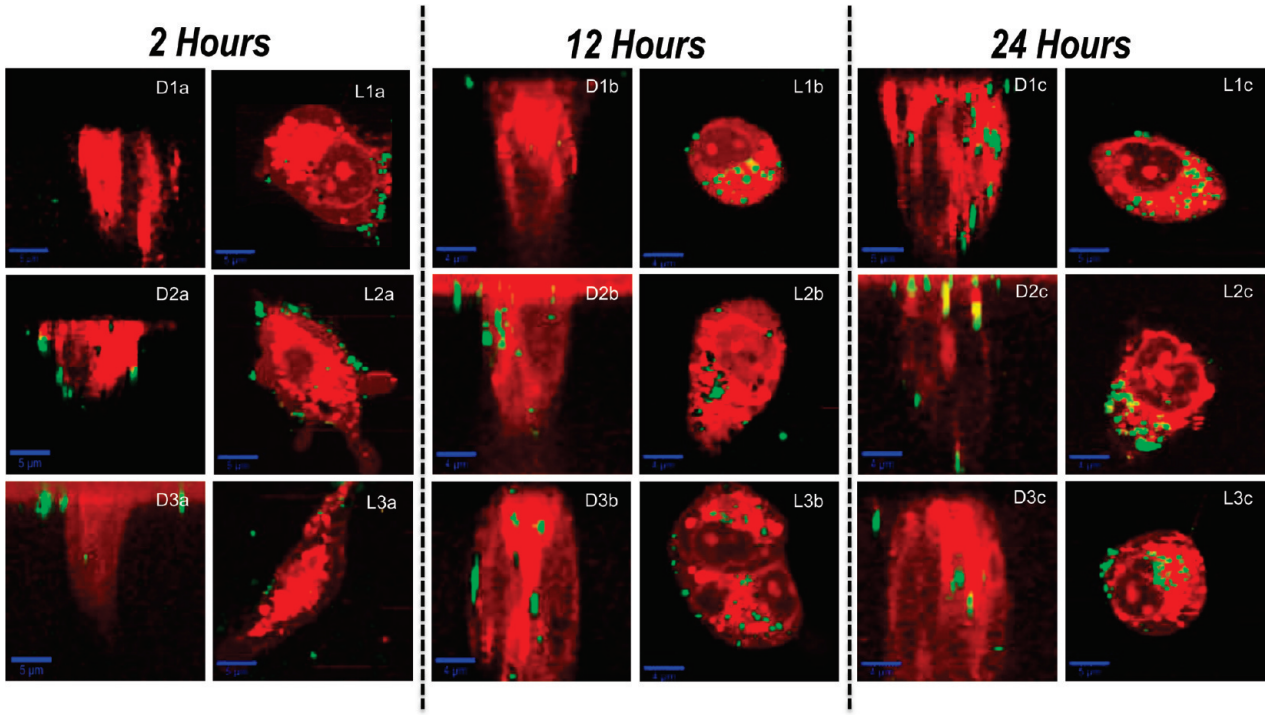

Figure 3. Dynamic imaging of cellular uptake of GNPs in LNCaP cells. Overlay images show relative uptake and localization of GNPs (green) at different time points in cells (red). 2 h: GNPs located at the cell membranes. 12 h: GNPs show intracellular uptake and are distributed in the cytoplasm. 24 h: GNPs located in the perinuclear region. D1−D3, depth scans of three different cells. L1−L3, lateral scans of corresponding cells in D1−D3. Letters a, b, and c correspond to 2, 12, and 24 h incubation. Three representative images are shown here per time point. For each time point, the experiment was carried out separately at least three times and two to three cell images were collected per experiment. (Scale bars = 5 μm.)

GNPs (for monodisperse GNPs see Figure 1b). Nevertheless, the trends in uptake and localization compare well with established methods (AES, TEM, and silver stain).

Discussion

GNP assisted molecular delivery and therapeutics are major evolving nanomedicine research areas.[43−46] GNPs are being used as effective delivery vehicles for drugs, genes or siRNA as well as other protein based ligands to the cell membrane, cytoplasm or nucleus. The GNP itself can also be used to more effectively deliver heat to the cell membrane and/or radiation at the cellular and subcellular level.[15,17] In these cases the dynamics and localization of the GNP within the cell (i.e., membrane, cytoplasm or nucleus) is critical to the intended therapeutic function. In order to study the GNP cell interactions critical to these events dynamically, a variety of methods have been and will continue to be utilized while CRM adds new capabilities. CRM, as shown here, takes advantage of the chemical information obtained from Raman spectra of the particles and the cell organic constituents to construct a spatial map of GNP cellular uptake and localization that is fast, label-free and at a high resolution of about ~250 nm.

Traditional methods of GNP localization such as TEM, histology and AES provide both quantitative and qualitative information on uptake, but are typically post-mortem, requiring considerable effort and time to perform fixation, embedding, staining (TEM and histology), or digestion of cells (AES). More recently, faster noninvasive optical methods for GNP assessment and cellular uptake have been developed which rely on optical properties of GNPs.[24,28−32,47] These include dark field, two-photon luminescence (TPL), multimodal photoacoustic, Rayleigh light scattering, fluorescence labeling of GNPs, and Raman approaches.[24,28−35] Some of these optical techniques require extensive equipment such

(43) Patra, C. R.; Bhattacharya, R.; Mukhopadhyay, D.; Mukherjee, P. Fabrication of gold nanoparticles for targeted therapy in pancreatic cancer. *Adv. Drug Delivery Rev.* **2010**, *62* (3), 346–361.

(44) Giljohann, D. A.; Seferos, D. S.; Daniel, W. L.; Massich, M. D.; Patel, P. C.; Mirkin, C. A. Gold Nanoparticles for Biology and Medicine. *Angew. Chem., Int. Ed.* **2010**, *49* (19), 3280–3294.

(45) Choi, C. H. J.; Alabi, C. A.; Webster, P.; Davis, M. E. Mechanism of active targeting in solid tumors with transferrin-containing gold nanoparticles. *Proc. Natl. Acad. Sci. U.S.A.* **2010**, *107* (3), 1235–1240.

(46) Cherukuri, P.; Glazer, E. S.; Curley, S. A. Targeted hyperthermia using metal nanoparticles. *Adv. Drug Delivery Rev.* **2010**, *62* (3), 339–345.

(47) Galanzha, E. I.; Kim, J.-W.; Zharov, V. P. Nanotechnology-based molecular photoacoustic and photothermal flow cytometry platform for *in-vivo* detection and killing of circulating cancer stem cells. *J. Biophotonics* **2009**, *2* (12), 725–735.

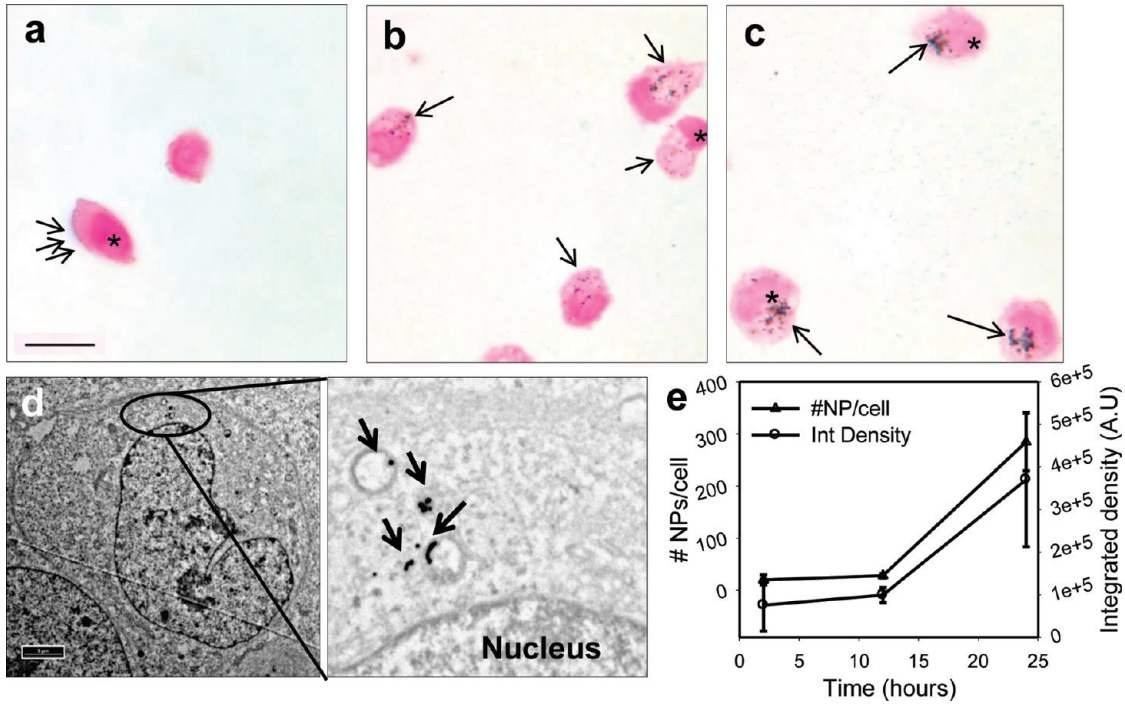

Figure 4. Corroborative studies of GNP uptake with histology, TEM and AES. (a, b, c) Histology images showing GNP uptake in LNCaP cells after 2, 12, and 24 h of treatment, respectively. Silver enhancement of GNPs shows up as black dots in histological sections counterstained with Fast Red (stars, nucleus; arrows, silver stained GNPs). (d) TEM micrograph of an LNCaP cell treated with GNPs for 24 h. Arrows in the close-up show clusters of GNPs (2−10 per cluster) in perinuclear space in membrane bound organelles. (e) Quantification of cellular uptake of GNPs as a function of time using AES and integrated density analysis of CRM images. The number of GNPs per cell increases with time with the biggest change between 12 and 24 h. Error bars, ±SD. AES analysis (left *y*-axis), $n = 3$. Integrated density analysis (right *y*-axis), $n = 3$ for 2 and 12 h, $n = 4$ for 24 h. (Histology scale bar = 10 μm, TEM scale bar =1 μm.)

as photoacoustics and two-photon approaches. Others such as dark field and Rayleigh light scattering are easy to set up, but their resolution is relatively poor and a separate fluorescent labeling of cells is necessary to colocalize particles.[28,31,35] In order to improve resolution and specificity, Raman approaches including SERS and CRM are now under active investigation.

Raman scattering originates from the inelastic interaction between a photon and a molecule, which changes its rotational or vibrational energy. A Raman spectrum is a plot of this change in energy with reference to the incident light (i.e., wavelength of a laser). Each Raman peak corresponds to a chemical bond in a certain vibrational mode of specific molecules,[48] and the peak intensity relates to the amount of the molecule present.[38] When this information is combined with the spatial information collected from the confocal microscope, a high resolution 2D or 3D chemical map can be generated that reveals the distribution of the molecule of interest in a given sample in a completely label-free manner.[49] Raman microscopy had suffered from weak signal intensity, low spatial resolution and long imaging time, mainly because of the weak nature of the Raman scattering. However, the recent development of CRM has enabled researchers to image biological systems much faster (seconds to minutes) with a resolution of ~200 nm (diffraction limit of the light).[49] CRM of liposomal and polymeric nanoparticles has been demonstrated in cells, due to the strong Raman effect from deuterated molecules or highly symmetric functional groups.[38] However, for metallic NPs such as GNPs, the use of Raman spectroscopy has been limited to SERS (surface enhanced Raman spectroscopy),[50,51] which requires special Raman active labels such as Rhodamine 6G,

(48) Chernenko, T.; Matthaus, C.; Milane, L.; Quintero, L.; Amiji, M.; Diem, M. Label-Free Raman Spectral Imaging of Intracellular Delivery and Degradation of Polymeric Nanoparticle Systems. *ACS Nano* **2009**, *3* (11), 3552–3559.

(49) Dong, J.; Hubel, A.; Bischof, J. C.; Aksan, A. Freezing-induced phase separation and spatial microheterogeneity in protein solutions. *J Phys Chem B* **2009**, *113* (30), 10081–10087.

(50) Keren, S.; Zavaleta, C.; Cheng, Z.; de la Zerda, A.; Gheysens, O.; Gambhir, S. S. Noninvasive molecular imaging of small living subjects using Raman spectroscopy. *Proc. Natl. Acad. Sci. U.S.A.* **2008**, *105* (15), 5844–5849.

(51) Qian, X.; Peng, X.-H.; Ansari, D. O.; Yin-Goen, Q.; Chen, G. Z.; Shin, D. M.; Yang, L.; Young, A. N.; Wang, M. D.; Nie, S. In vivo tumor targeting and spectroscopic detection with surface-enhanced Raman nanoparticle tags. *Nat. Biotechnol.* **2008**, *26* (1), 83–90.

DSNB, or malachite green isothiocyanate[32,50−52] to be tagged on the surface of GNPs. Thus, approaches that can track GNPs using Raman without SERS labels by CRM may yield important advantages.

The Raman spectrum of the concentrated GNP solution shows several peaks (Figure 1a). These include a photoluminescence (PL) peak (180−1800 cm^{-1}) attributable to the excitation of their surface plasmons by Raman laser, OH bending and stretching peaks (at 1600 cm^{-1} and 2800−3800 cm^{-1} respectively) due to solvent (water), and CH stretching peak from PEG.[36,53] The intensity of the PL peak shows a linear correlation with the concentration of the GNPs in DI water (Figure 1b). GNPs in solution are monodisperse, which explains the linearity of the correlation; however, GNPs in endocytic or lysosomal vesicles appear as small clusters (see below, Figure 4), which makes the absolute quantification of GNPs using this method challenging. Despite this, CRM imaging offers reliable information on cellular binding, uptake and intracellular localization of GNPs in a matter of minutes that is comparable to the best available techniques (i.e., dark field or SERS) in a noninvasive and label-free manner with minimal sample preparation or specialized equipment settings.

A typical cell scan using CRM takes about 10−12 min depending upon the pixel resolution desired. For example, cell images in Figure 2 and 3 each have 80 × 80 pixel resolution (10 min) and were generated using the C−H peak at 2800−3100 cm^{-1} (representing organic components, see Figure 2h). A higher resolution scan (such as 100 × 100 pixels, ∼16 min) makes identification of the nucleus and other organelles easier. A Raman scan over a number of cells with sufficient sensitivity to PL peaks may be done within 1−2 min. With such quick analysis and limited sample preparation, cellular biodistribution of different GNP embodiments can be made even easier and faster. For instance, whether a GNP is taken up and located within the cell can be easily determined as a function of different coating, charge or targeting using CRM in a given cell type (see Figure 1 in the Supporting Information).

In order to show that CRM imaging can provide dynamic uptake information for a model GNP system, experiments were performed at 2, 12, and 24 h after incubation of cells with GNPs. These time points were chosen so that uptake data obtained from CRM can be compared with our own AES and TEM studies as well as other such studies available in the literature.[27,41,42] After the 2 h treatment and washing of excess GNPs, most GNPs were found to be at the cell periphery as seen in cells L1a and L2a (Figure 3), with little intracellular uptake (L3a of Figure 3). The size of the NPs has been shown to affect the uptake process.[19] Membrane bound GNPs seem to be forming clusters judging from the size of the green spots in these images (Figure 3, 2 h). For 30 nm GNPs, it has been shown that such clusters are about 100−200 nm in size[41] and contain about 7−8 NPs per cluster.[20] It has been suggested that NPs with ∼55 nm size have the fastest membrane wrapping time thereby enough free energy to drive NPs into a cell, whereas NPs smaller than that do not produce enough free energy to be wrapped individually by cell membrane and thus cluster together.[19,54] For NPs that contain a ligand on their surface, such binding events may be different due to the receptor mediated endocytosis (see Figure 1 in the Supporting Information). Incubation of cells with GNPs for 12 h at 37 °C shows GNP clusters distributed throughout the cytoplasm. From 12 to 24 h, the uptake continues with growing cluster size of GNPs and their localization near the nucleus. The perinuclear localization at 24 h agrees with data on GNP incubation with BeWo cells[42] and the expected pathway for lysosomal internalization in macrophages.[27] The uptake kinetics and intracellular distribution of GNPs in this study are consistent with the pinocytotic pathway of endocytosis of nontargeted (i.e., PEGylated) GNPs.[27] These results were further confirmed using histology and TEM, which are the most widely accepted methods to study GNP uptake. Since we did not look at time points beyond 24 h, it is not clear whether the GNPs in perinuclear space would enter the nucleus. For successful delivery of NPs to cell nucleus certain requirements have to be met: (1) size <30 nm, (2) receptor mediated endocytosis, (3) escape from endosomal/lysosomal pathway, and (4) nuclear localization signal (NLS).[1] Since GNPs used in this study are 30 nm in core diameter with hydrodynamic diameter of approximately 60 nm, and they lack specific functionalization for nuclear targeting, we do not expect the GNPs to enter the nucleus even at longer time points.

ICP-AES and MS are used as benchmark quantitative techniques for GNP cellular and tissue uptake.[19,20,55] There are about 19.9 ± 0.97, 28.0 ± 0.44, 284 ± 5.5 GNPs per cell at 2, 12, and 24 h respectively, and cellular uptake does not reach saturation according to the AES data (Figure 4e). GNPs of 14 and 50 nm diameter and negative surface charge show an uptake of about 2000−2500 GNPs/cell at 2 h when incubated with a 4−16 μM GNP concentration, and they reach saturation in uptake by 10 h.[20] In this case, 0.19 nM final concentration of GNP was used, so it is expected that the uptake would be much lower at any given time point. An integrated density analysis of images created with PL

(52) Porter, M. D.; Lipert, R. J.; Siperko, L. M.; Wang, G.; Narayanan, R. SERS as a bioassay platform: fundamentals, design, and applications. *Chem. Soc. Rev.* **2008**, *37* (5), 1001–1011.

(53) Morais, P. C.; da Silva, S. W.; Soler, M. A. G.; Sousa, M. H.; Tourinho, F. A. Raman study of ionic water-based copper and zinc ferrite magnetic fluids. *J. Magn. Magn. Mater.* **1999**, *201* (1−3), 105–109.

(54) Bao, G.; Bao, X. R. Shedding light on the dynamics of endocytosis and viral budding. *Proc. Natl. Acad. Sci. U.S.A.* **2005**, *102* (29), 9997–9998.

(55) Balasubramanian, S. K.; Jittiwat, J.; Manikandan, J.; Ong, C.-N.; Yu, L. E.; Ong, W.-Y. Biodistribution of gold nanoparticles and gene expression changes in the liver and spleen after intravenous administration in rats. *Biomaterials* **2009**, *31* (8), 2034–2042.

peak intensities (i.e., Figure 2d,e) can be used as a semiquantitative method to compare to AES data for cellular uptake of GNPs at 2, 12, and 24 h, and shows a similar trend in uptake as AES (Figure 4e). This semiquantitative information in conjunction with the CRM images is an advantage of this technique for the rapid study of cellular uptake and localization of GNP constructs. Precise quantification of number of GNPs per cluster based on the PL peak intensity is challenging as the clustering of GNPs may influence the peak intensity in a nonlinear way. However, it may be possible in future studies to determine the number of GNPs in a cluster using the concept of "plasmon ruler" assuming cluster sizes and/or distance between nanoparticles remain relatively constant.[56]

The method presented here can be used for the purpose of screening different GNP embodiments in various cell types for their cellular attachment, uptake and general localization, at various time points and incubation conditions. For example, if a therapeutic molecule is being designed for membrane or intracellular (but not nuclear) delivery using the GNP as a carrier, or if a GNP is being designed to specifically target the nucleus, different prototypes of this molecule can be tested rapidly using this method. Specifically, the dynamics of uptake, cellular localization and delivery efficiency in one or more cell types of interest can be rapidly determined. In this way, this method has the potential to facilitate high-throughput chip based Raman screening to test multiple conditions simultaneously.

Acknowledgment. Financial support was provided by the Center for Nanostructured Applications (CNA) and the NSF MRSEC Seed Grant at the University of Minnesota. We wish to thank W. C. W. Chan at the University of Toronto for useful discussions and A. Ressler at the Characterization Facility for help with TEM methods. GNPs were a gift from CytImmune Sciences Inc. (Rockville, MD). Part of this work was carried out in the College of Science and Engineering Characterization Facility, a member of the NSF-funded Materials Research Facility Network (www.mrfn.org).

Supporting Information Available: CRM images depicting cellular uptake of tumor necrosis factor (TNF) coated GNP and negatively charged GNPs as mentioned in text. This material is available free of charge via the Internet at http://pubs.acs.org.

MP1002587

(56) Sonnichsen, C.; Reinhard, B. M.; Liphardt, J.; Alivisatos, A. P. A molecular ruler based on plasmon coupling of single gold and silver nanoparticles. *Nat. Biotechnol.* **2005**, *23* (6), 741–745.